Hindawi Publishing Corporation
Journal of Nanomaterials
Volume 2015, Article ID 346086, 6 pages
http://dx.doi.org/10.1155/2015/346086

Research Article

Facile Synthesis of Highly Dispersed $WO_3 \cdot H_2O$ and WO_3 Nanoplates for Electrocatalytic Hydrogen Evolution

Wen-Hui Hu,[1] Guan-Qun Han,[1,2] Bin Dong,[1,2] and Chen-Guang Liu[1]

[1]*State Key Laboratory of Heavy Oil Processing, China University of Petroleum (East China), Qingdao 266580, China*
[2]*College of Science, China University of Petroleum (East China), Qingdao 266580, China*

Correspondence should be addressed to Bin Dong; dongbin@upc.edu.cn and Chen-Guang Liu; cgliu.upc.edu.cn@gmail.com

Received 9 December 2014; Accepted 17 January 2015

Academic Editor: Chunyi Zhi

The highly dispersed $WO_3 \cdot H_2O$ nanoplates have been synthesized by a facile hydrothermal reaction assisted by citrate acid. WO_3 nanoplates have been prepared by the calcination of as-prepared $WO_3 \cdot H_2O$ at 450°C. XRD data show that $WO_3 \cdot H_2O$ and WO_3 have good crystal structure and high purity. SEM images show that $WO_3 \cdot H_2O$ and WO_3 have the uniform nanoplates morphology with the edge length of about 100–150 nm. The selective absorbance of citrate acid with many OH groups onto [010] facet of tungsten oxide precursors can result in the controlled growth of $WO_3 \cdot H_2O$, thus leading to the good dispersion and small size of $WO_3 \cdot H_2O$ nanoplates. The electrocatalytic activity of $WO_3 \cdot H_2O$ and WO_3 for hydrogen evolution reaction (HER) has been investigated in detail. The good electrocatalytic activity for HER has been obtained, which may be attributed to the good dispersion and small size of nanoplates. And the growth mechanisms of $WO_3 \cdot H_2O$ and WO_3 nanoplates have been discussed.

1. Introduction

Hydrogen evolution reaction has attracted the growing interest because hydrogen as a promising sustainable energy carrier could accelerate the transition from the hydrocarbon economy to sustainable energy economy [1]. One of the promising fashions of hydrogen production is to adopt electrochemical [2] route. Novel metals such as Pt are the highly active electrocatalysts for HER [3], but the disadvantages of Pt are high cost and limited reserve, preventing the utilization of novel metal electrocatalysts. Therefore, designing the earth-abundant elements as active electrocatalysts represents future development of the electrocatalysts for HER [4].

As important *n*-type semiconductors, tungsten oxide hydrates ($WO_3 \cdot nH_2O$) and tungsten oxides (WO_3) have obtained more and more attention due to their polytypic structures and excellent physical/chemical properties [5]. Many applications have been extensively investigated such as lithium-ion batteries [6], supercapacitors [7], gas sensors [8], photocatalysts [9, 10], solar energy devices [11], and electrocatalyst in electrolysis of water for HER [12]. Furthermore, the monoclinic WO_3 is more stable phase than any other WO_3 structures owing to the structure consisting of a three-dimensional network of WO_6 octahedrons [13, 14].

Up to now, many approaches have been adopted to synthesize WO_3 nanostructures with different morphologies including nanotubes [15], nanowires [16], nanorods [17], nanoplates [18], and hollow spheres [19]. Among the different morphologies, nanoplate-like structure displays excellent gas response and catalytic properties because of their high density of surface sites [20]. $WO_3 \cdot nH_2O$ has been usually prepared through the liquid-phase synthesis routes, and WO_3 has been synthesized by annealing $WO_3 \cdot nH_2O$ to remove crystal water. The hydrothermal method can be used owing to some advantages in controlling the morphology, size, and homogeneity at the mild temperature for large-scale production [21]. However, developing a facile route for large-scale production of WO_3 with high crystal phase and high purity is still a challenge.

In our work, highly dispersed $WO_3 \cdot H_2O$ nanoplates have been synthesized by a facile hydrothermal reaction assisted by citrate acid. WO_3 nanoplates have also been prepared by the calcination of $WO_3 \cdot H_2O$ at 450°C for 4 h. SEM images show that as-prepared $WO_3 \cdot H_2O$ and WO_3 samples have the uniform nanoplates morphology with the edge length

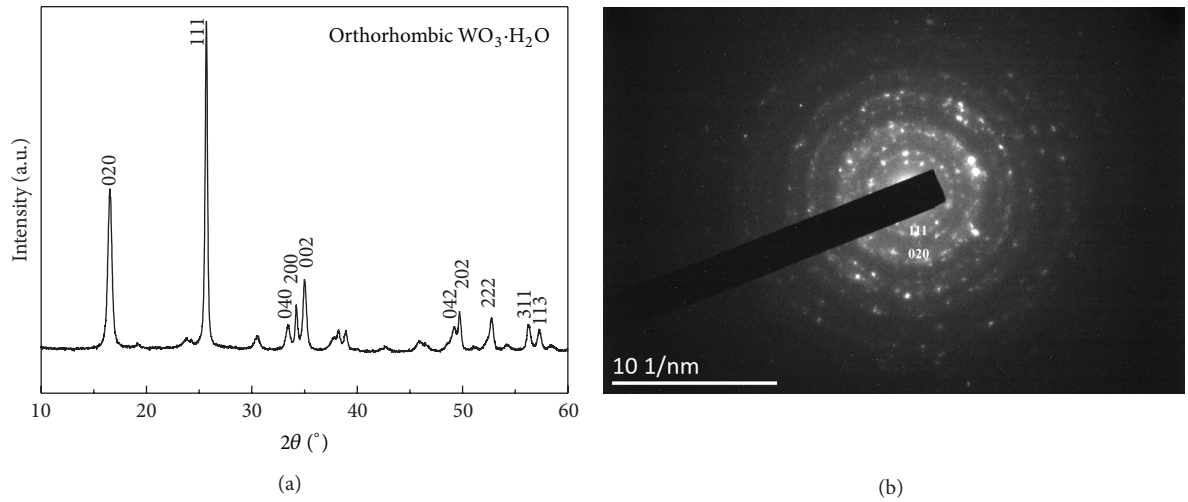

Figure 1: (a) XRD patterns of $WO_3 \cdot H_2O$ as-prepared by hydrothermal method. (b) Selected area electron diffraction (SAED) patterns of $WO_3 \cdot H_2O$.

of about 100–150 nm. The electrocatalytic activity of the two samples for HER properties has been investigated in detail. The good electrocatalytic activity for HER has been obtained, which may be attributed to the good dispersion and small size of nanoplates. And the growth mechanisms of highly dispersed $WO_3 \cdot H_2O$ and WO_3 nanoplates have been discussed.

2. Experimental

2.1. Preparation of $WO_3 \cdot H_2O$ and WO_3 Nanoplates. All chemical reagents were of analytic purity and used directly without further purification. $WO_3 \cdot H_2O$ nanoplates have been prepared by dissolving 0.4 g citrate acid and 0.53 g $Na_2WO_4 \cdot 2H_2O$ in 40 mL deionized water in order under stirring. The pH value of the solution was adjusted to about 1.0 by the addition of HCl. Then the mixture was transferred into a 50 mL Teflon-lined stainless steel autoclave and sealed, and the autoclave was placed in a preheated oven at 120°C for 3 h. After being naturally cooled down to room temperature, the yellow precipitates were collected by filtration and washed with deionized water and ethanol for several times and dried in oven at 80°C. The as-prepared $WO_3 \cdot H_2O$ nanoplates have been calcined at 450°C for 4 h to prepare WO_3 samples. The yellow $WO_3 \cdot H_2O$ samples changed to white-yellow WO_3 samples.

2.2. Characterization of Morphology and Structure. Crystallographic structure of all as-prepared samples was investigated with X-ray powder diffraction (XRD, X'Pert PRO MPD, Cu KR) at a scanning rate of $8^\circ C\,min^{-1}$. XRD data were collected in the 2θ ranges from 10 to 60°. The morphology of the samples was examined with field-emission scanning electron microscopy (SEM, Hitachi, S-4800). Selected area electron diffraction (SAED) was used to examine samples' crystallinity (TEM, JEM-2100UHR with an accelerating voltage of 200 kV).

2.3. Electrochemical Measurement. The glassy carbon electrode (geometric surface area of glassy carbon = $0.1256\,cm^2$), Pt plate, and Ag/AgCl electrode were used as working, counter, and reference electrodes, respectively. 0.5 M H_2SO_4 solution was used as electrolyte for linear sweep voltammetry and electrochemical impedance spectra on the Gamry reference 600 electrochemical workstation. The working electrodes were prepared by catalytic ink-dispersing 20 mg catalyst in 1 mL ethanol and 0.01 mL of 5 wt% Nafion under 30 min ultrasonic radiation.

3. Results and Discussion

Figure 1 displays XRD patterns and SAED patterns of $WO_3 \cdot H_2O$ synthesized by hydrothermal route. As shown in Figure 1(a), all the peaks clearly demonstrate that the samples are the orthorhombic $WO_3 \cdot H_2O$ crystal, corresponding to the (020), (111), and (002) diffraction at 2θ of 16.5°, 25.7°, and 35.1° (JCPDS number 43-0679 with lattice constants of $a = 0.5238$ nm, $b = 0.1070$ nm, and $c = 0.5120$ nm). The high intensity and narrow peaks of (020) and (111) mean good crystallinity of $WO_3 \cdot H_2O$. No other impurity peaks can be observed from the patterns, indicating high purity of the sample. It can be concluded that the hydrothermal process assisted by citrate acid could produce the pure $WO_3 \cdot H_2O$ with the orthorhombic phase. Figure 1(b) shows the corresponding SAED patterns of $WO_3 \cdot H_2O$, indicating that these nanoplates have a polycrystalline orthorhombic $WO_3 \cdot H_2O$ phase.

To investigate the morphology and size of $WO_3 \cdot H_2O$, the as-prepared samples have been measured by SEM (in Figure 2). As shown in Figure 2(a), SEM images of $WO_3 \cdot H_2O$ assisted by citrate acid show the uniform nanoplates morphology with the edge length of about 100–150 nm. With higher magnification, it can be seen from Figure 2(b) that the thickness of each $WO_3 \cdot H_2O$ nanoplate is about 30 nm. The coarse surface and monodispersed structure of

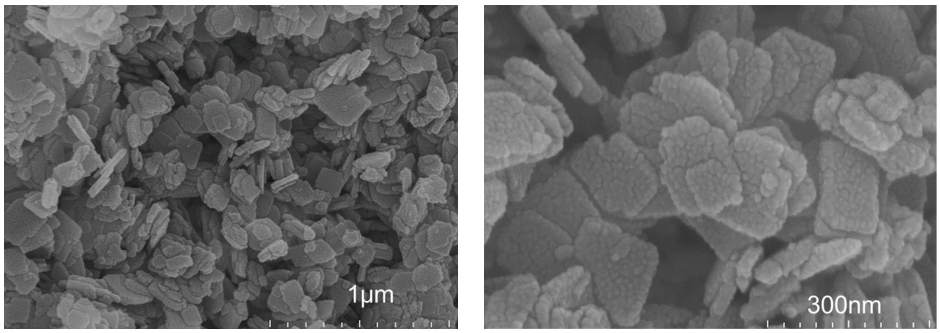

(a) (b)

Figure 2: SEM images of $WO_3 \cdot H_2O$ nanoplates.

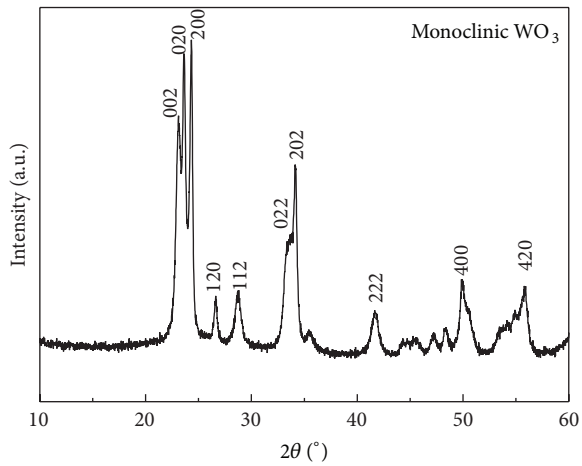

Figure 3: XRD patterns of WO_3 after being calcined in 450°C for 4 h.

Table 1: BET area of $WO_3 \cdot H_2O$ and WO_3 nanoplates.

Materials	$WO_3 \cdot H_2O$	WO_3
BET area ($m^2 \cdot g^{-1}$)	23.28	11.99

$WO_3 \cdot H_2O$ nanoplates can also be clearly observed, which maybe indicate the lager specific surface area and more active sites for HER [12]. From Table 1, it can be seen that $WO_3 \cdot H_2O$ nanoplates have much higher Brunauer-Emmett-Teller (BET) specific surface area of 23.28 $m^2 \cdot g^{-1}$ than WO_3 nanoplates (11.99 $m^2 \cdot g^{-1}$), which implies that the BET area of WO_3 nanoplates is decreased after the calcination.

XRD patterns of WO_3 after calcination at 450°C are shown in Figure 3. It can be seen that all the diffraction peaks of WO_3 samples are consistent with the monoclinic WO_3 phase (JCPDS number 43-1035). No other peaks from XRD patterns were detected, indicating that $WO_3 \cdot H_2O$ samples completely transform to the pure WO_3 phase with three distinct diffraction peaks of (002), (020), and (200), respectively.

The SEM images of the calcined WO_3 samples are shown in Figure 4. It can be found in Figure 4(a) that the similar nanoplates morphology has been maintained during the process of calcination at 450°C. However, the surface of WO_3 nanoplates obviously becomes smooth, which may be attributed to the elimination of water molecules between the tungstite layers. Figure 4(b) shows that some aggregation growth of WO_3 nanoplates appears with the slight increasing of thickness of WO_3 nanoplates due to the effect of the calcination process at 450°C.

The transformation process from $WO_3 \cdot H_2O$ nanoplates to WO_3 nanoplates is illustrated in Figure 5. Firstly, H_2WO_4 phase formed when adding HCl into Na_2WO_4 solution (1) as follows:

$$Na_2WO_4 + 2HCl \longrightarrow H_2WO_4 + 2NaCl \quad (1)$$

$$H_2WO_4 \longrightarrow WO(OH)_4(OH_2) \quad (2)$$

Secondly, H_2WO_4 precursor changed to $[WO(OH)_4(OH_2)]$ (2), with the sixfold coordinated W^{6+} including one oxygen atom and water molecule along *b*-axis, two OH groups along *a*-axis, and two OH groups along *c*-axis, respectively (as shown in Figure 5(a)). Thirdly, during hydrothermal process, $[WO(OH)_4(OH_2)]$ converted to the octahedral $[WO_5(OH_2)]$ layer by oxolation, which is the structural unit of $WO_3 \cdot H_2O$ with more OH on the [010] facets [9]. There are stable hydrogen bonds force-derived from the terminal oxygen atoms and coordinated water molecules between the neighbouring layers of $WO_3 \cdot H_2O$, thus leading to the formation of $WO_3 \cdot H_2O$ with layers structure (Figure 5(b)). When being calcined at 450°C, the water molecules between the neighbouring layers of $WO_3 \cdot H_2O$ have been released with keeping the layer structure. The dehydration process has been proved to be a topotactic process [22]. Finally, the structure of monoclinic WO_3 is obtained in Figure 5(c). During the hydrothermal process, the growth of $WO_3 \cdot H_2O$ nanoplates has largely been affected by the citrate acid as dispersant and control agent. Similar research has been reported that certain crystal faces of WO_3 can be impeded by using that preferentially adsorbed to specific crystal faces with the assistance of malic acid [23]. In our work, citrate acid including many OH groups can be selectively absorbed onto [010] facet because there are many OH groups on the surface of $[WO_5(OH_2)]$ layer. The selective absorbance may be attributed to the strong interaction between the OH groups (Figure 5(d)). Therefore, the stacking growth along (010) facet has been controlled by the adding of citrate acid. And the

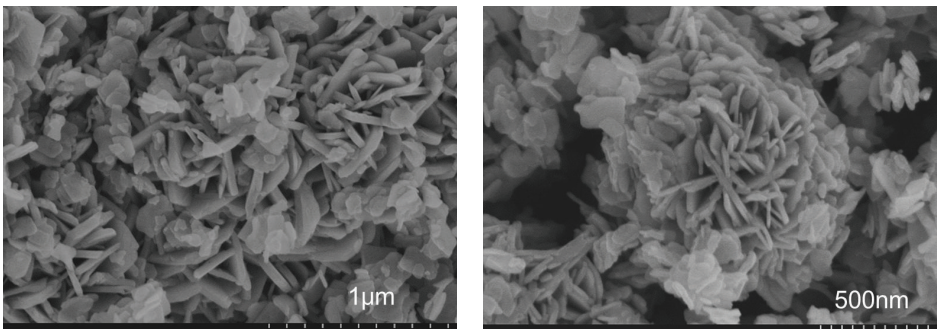

(a) (b)

Figure 4: SEM images of WO_3 nanoplates.

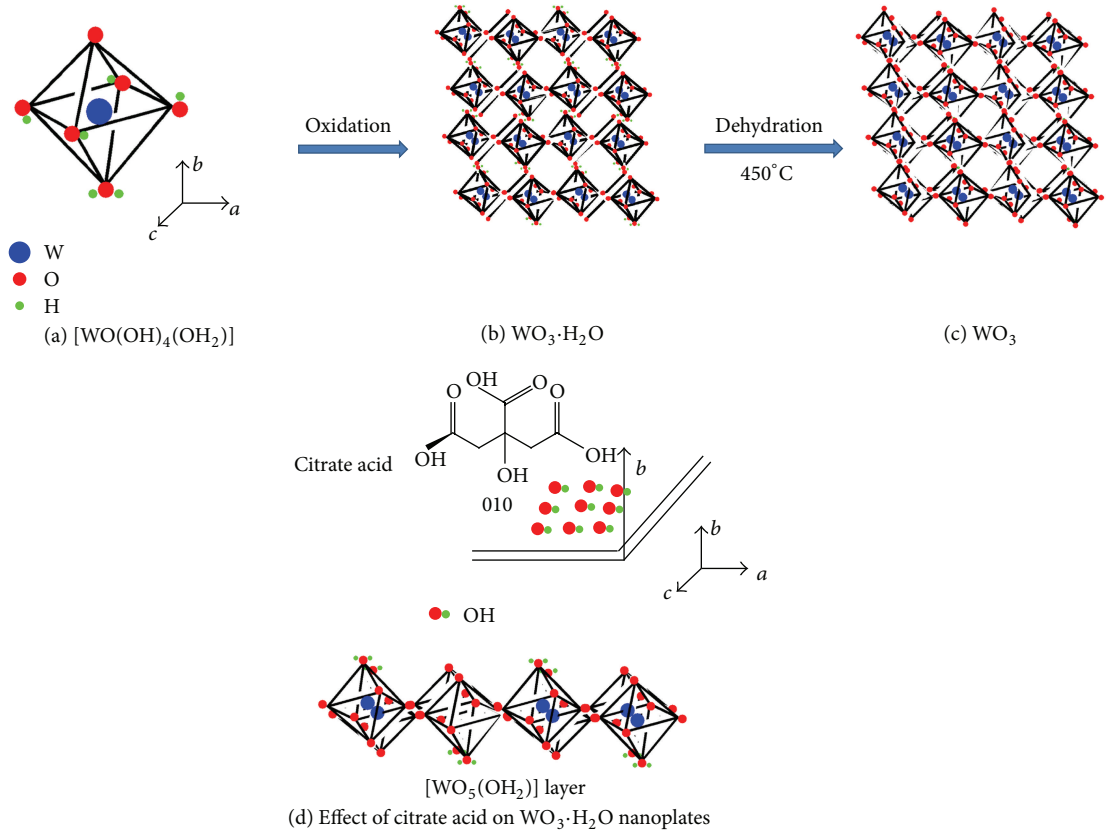

Figure 5: Schematic illustration of the formation mechanism of WO_3 nanoplates.

good dispersion and small size of $WO_3 \cdot H_2O$ nanoplates could be obtained.

The electrocatalytic activity for HER of $WO_3 \cdot H_2O$ and WO_3 nanoplates has been studied in 1 M H_2SO_4 solution over the potential range of −0.60 to +0.8 V at a scan rate of 50 mVs^{-1} by the linear sweep voltammetry (LSV), Tafel plots, and electrochemical impedance spectra. Figure 6 shows the LSV curves and Tafel plots of $WO_3 \cdot H_2O$ and WO_3 nanoplates. It can be seen from Figure 6(a) that $WO_3 \cdot H_2O$ exhibits the electrocatalytic activity for HER with onset potential of −0.20 V (versus RHE) and the exchange current density of −4.5 mA cm^{-2} at overpotential of 300 mV. The onset potential for the HER of WO_3 nanoplates is about −0.09 V. The exchange current density of WO_3 sample is about −7.5 mA cm^{-2} at overpotential of 300 mV.

Figure 6(b) shows Tafel slopes of 97 and 101 mV dec^{-1} for $WO_3 \cdot H_2O$ and WO_3 nanoplates, respectively. The ideal electrocatalysts should have low Tafel slopes and high cathodic current densities. For example, Pt has a high current density in the order of 10^{-3} A cm^{-2} and a Tafel slope of 30 mV dec^{-1} for HER. However, in our work, WO_3 nanoplates have a higher current density but a higher Tafel slope than that of $WO_3 \cdot H_2O$. According to the previous report [24], which electrocatalyst is better depends on the targeted current

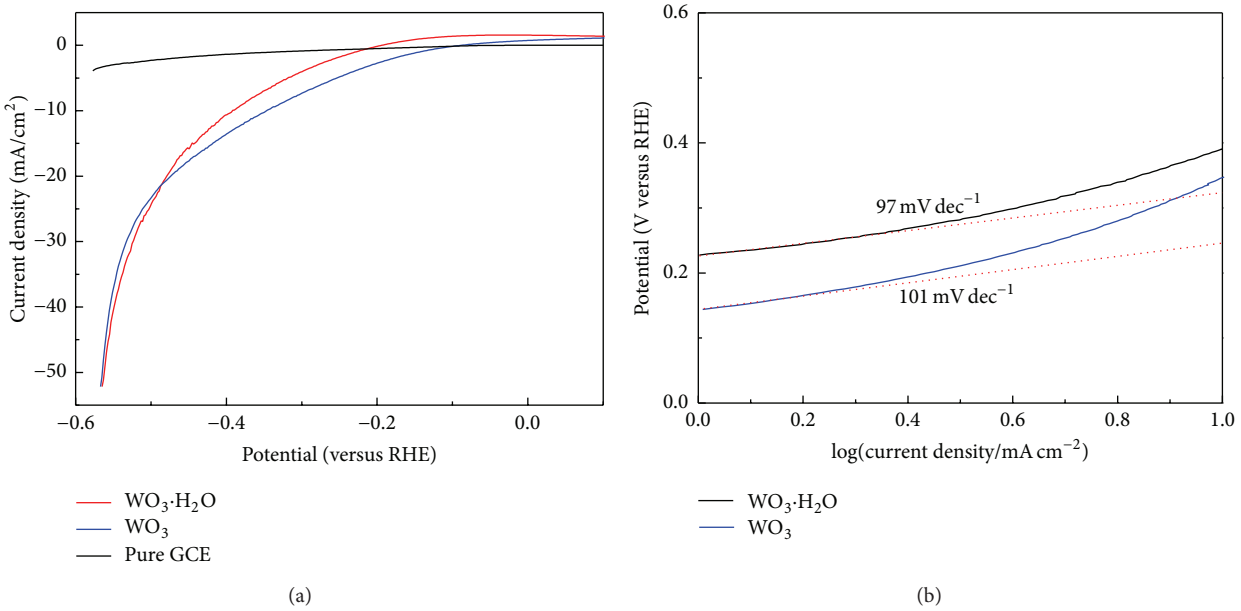

FIGURE 6: (a) Linear sweep voltammogram curves of $WO_3 \cdot H_2O$ and WO_3 nanoplates. (b) Tafel plots of $WO_3 \cdot H_2O$ and WO_3 nanoplates.

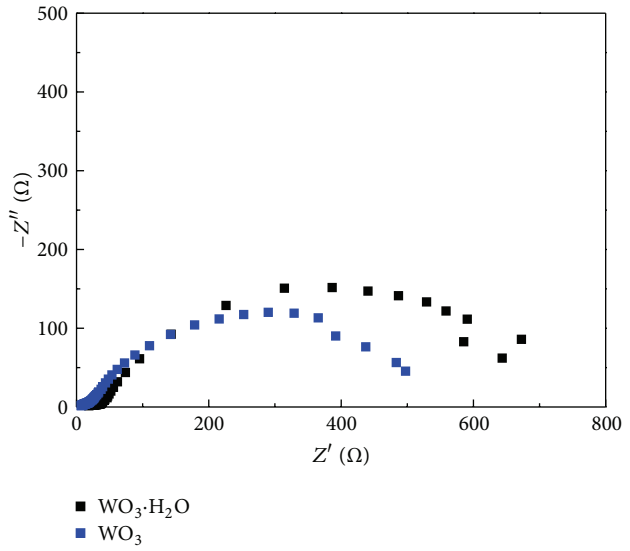

FIGURE 7: Electrochemical impedance spectra of $WO_3 \cdot H_2O$ and WO_3 nanoplates.

density. For example, to obtain the targeted current density of 10 mA cm^{-2}, $WO_3 \cdot H_2O$ sample requires −390 mV of overpotential, while WO_3 sample requires −340 mV. Therefore, WO_3 is the better electrocatalyst for HER.

The electrochemical impedance spectra of the two different samples can be shown in Figure 7. WO_3 sample shows the smaller charge-transfer resistance than $WO_3 \cdot H_2O$, which implies that WO_3 has much faster electron transfer and improved efficiency for HER than $WO_3 \cdot H_2O$. The enhancement of conductivity also benefits from the compact structure of WO_3 after calcination at high temperature. The poor HER activity of $WO_3 \cdot H_2O$ may be attributed to the existence of crystal H_2O. Firstly, the crystal H_2O may occupy some active sites for HER, resulting in poor catalytic activity. Secondly, the poor conductivity of $WO_3 \cdot H_2O$ impedes the transportation of the electrons between the active sites and the electrode. So $WO_3 \cdot H_2O$ has the worse HER activity than WO_3.

4. Conclusions

The highly dispersed $WO_3 \cdot H_2O$ and WO_3 nanoplates have been synthesized by a facile process assisted by citrate acid. The as-prepared $WO_3 \cdot H_2O$ and WO_3 have the uniform nanoplates morphology with good crystal structure and high purity, which may be attributed to the adding of citrate acid. The selective absorbance of citrate acid onto [010] facet of $[WO_5(OH_2)]$ layer may result in the good dispersion and small size of $WO_3 \cdot H_2O$ nanoplates. The electrocatalytic activity of $WO_3 \cdot H_2O$ and WO_3 for HER has been studied. The poor electrocatalytic activity of $WO_3 \cdot H_2O$ compared to WO_3 may be attributed to the existence of crystal H_2O.

Conflict of Interests

The authors declare that there is no conflict of interests regarding the publication of this paper.

Acknowledgment

This work is financially supported by the National Natural Science Foundation of China (no. U1162203).

References

[1] M. S. Dresselhaus and I. L. Thomas, "Alternative energy technologies," *Nature*, vol. 414, no. 6861, pp. 332–337, 2001.

[2] Z. Chen, A. J. Forman, and T. F. Jaramillo, "Bridging the gap between bulk and nanostructured photoelectrodes: The impact of surface states on the electrocatalytic and photoelectrochemical properties of MoS2," *Journal of Physical Chemistry C*, vol. 117, no. 19, pp. 9713–9722, 2013.

[3] J. K. Nørskov, T. Bligaard, A. Logadottir et al., "Trends in the exchange current for hydrogen evolution," *Journal of the Electrochemical Society*, vol. 152, no. 3, pp. J23–J26, 2005.

[4] H. Vrubel and X. L. Hu, "Molybdenum boride and carbide catalyze hydrogen evolution in both acidic and basic solutions," *Angewandte Chemie—International Edition*, vol. 51, no. 51, pp. 12703–12706, 2012.

[5] C. A. Bignozzi, S. Caramori, V. Cristino, R. Argazzi, L. Meda, and A. Tacca, "Nanostructured photoelectrodes based on WO_3: applications to photooxidation of aqueous electrolytes," *Chemical Society Reviews*, vol. 42, no. 6, pp. 2228–2246, 2013.

[6] W. Li and Z. Fu, "Nanostructured WO_3 thin film as a new anode material for lithium-ion batteries," *Applied Surface Science*, vol. 256, pp. 2447–2452, 2010.

[7] M. S. Zhu, W. J. Meng, Y. Huang, Y. Huang, and C. Y. Zhi, "Proton-insertion-enhanced pseudocapacitance based on the assembly structure of tungsten oxide," *ACS Applied Materials & Interfaces*, vol. 6, no. 21, pp. 18901–18910, 2014.

[8] C. Zhang, A. Boudiba, P. De Marco, R. Snyders, M.-G. Olivier, and M. Debliquy, "Room temperature responses of visible-light illuminated WO_3 sensors to NO_2 in sub-ppm range," *Sensors and Actuators B*, vol. 181, pp. 395–401, 2013.

[9] J. Yang, W. Li, J. Li, D. Sun, and Q. Chen, "Hydrothermal synthesis and photoelectrochemical properties of vertically aligned tungsten trioxide (hydrate) plate-like arrays fabricated directly on FTO substrates," *Journal of Materials Chemistry*, vol. 22, no. 34, pp. 17744–17752, 2012.

[10] S. S. Thind, M. Tian, and A. Chen, "Direct growth and photoelectrochemical study of WO_3 nanostructured materials," *Electrochemistry Communications*, vol. 43, pp. 13–17, 2014.

[11] H. D. Zheng, Y. Tachibana, and K. Kalantar-Zadeh, "Dye-sensitized solar cells based on WO_3," *Langmuir*, vol. 26, no. 24, pp. 19148–19152, 2010.

[12] D. J. Ham, A. Phuruangrat, S. Thongtem, and J. S. Lee, "Hydrothermal synthesis of monoclinic WO_3 nanoplates and nanorods used as an electrocatalyst for hydrogen evolution reactions from water," *Chemical Engineering Journal*, vol. 165, no. 1, pp. 365–369, 2010.

[13] C. Guéry, C. Choquet, F. Dujeancourt, J. M. Tarascon, and J. C. Lassègues, "Infrared and X-ray studies of hydrogen intercalation in different tungsten trioxides and tungsten trioxide hydrates," *Journal of Solid State Electrochemistry*, vol. 1, no. 3, pp. 199–207, 1997.

[14] X. Li, G. Zhang, F. Cheng, B. Guo, and J. Chen, "Synthesis, characterization, and gas-sensor application of WO_3 nanocuboids," *Journal of the Electrochemical Society*, vol. 153, no. 7, pp. H133–H137, 2006.

[15] M. Schieder, T. Lunkenbein, T. Martin, W. Milius, G. Auffermann, and J. Breu, "Hierarchically porous tungsten oxide nanotubes with crystalline walls made of the metastable orthorhombic polymorph," *Journal of Materials Chemistry A*, vol. 1, no. 2, pp. 381–387, 2013.

[16] A. Phuruangrat, D. J. Ham, S. J. Hong, S. Thongtem, and J. S. Lee, "Synthesis of hexagonal WO_3 nanowires by microwave-assisted hydrothermal method and their electrocatalytic activities for hydrogen evolution reaction," *Journal of Materials Chemistry*, vol. 20, no. 9, pp. 1683–1690, 2010.

[17] J. Zhu, S. L. Wang, S. H. Xie, and H. X. Li, "Hexagonal single crystal growth of WO_3 nanorods along a [110] axis with enhanced adsorption capacity," *Chemical Communications*, vol. 47, no. 15, pp. 4403–4405, 2011.

[18] H. Zhang, G. Duan, Y. Li, X. Xu, Z. Dai, and W. Cai, "Leaf-like tungsten oxide nanoplatelets induced by laser ablation in liquid and subsequent aging," *Crystal Growth and Design*, vol. 12, no. 5, pp. 2646–2652, 2012.

[19] Y. Liu, Q. Li, S. Gao, and J. K. Shang, "Template-free solvothermal synthesis of $WO_3/WO_3{\cdot}H_2O$ hollow spheres and their enhanced photocatalytic activity from the mixture phase effect," *CrystEngComm*, vol. 16, no. 32, pp. 7493–7501, 2014.

[20] X. Su, Y. Li, J. Jian, and J. Wang, "In situ etching WO_3 nanoplates: hydrothermal synthesis, photoluminescence and gas sensor properties," *Materials Research Bulletin*, vol. 45, pp. 1960–1963, 2010.

[21] J. Polleux, A. Gurlo, N. Barsan, U. Weimar, M. Antonietti, and M. Niederberger, "Template-free synthesis and assembly of single-crystalline tungsten oxide nanowires and their gas-sensing properties," *Angewandte Chemie—International Edition*, vol. 118, no. 2, pp. 267–271, 2006.

[22] J. M. Ma, J. Zhang, S. R. Wang et al., "Topochemical preparation of WO_3 nanoplates through precursor H_2WO_4 and their gas-sensing performances," *The Journal of Physical Chemistry C*, vol. 115, no. 37, pp. 18157–18163, 2011.

[23] Z.-Y. Jiang, Q. Kuang, Z.-X. Xie, and L.-S. Zheng, "Syntheses and properties of micro/nanostructured crystallites with high-energy surfaces," *Advanced Functional Materials*, vol. 20, no. 21, pp. 3634–3645, 2010.

[24] C. G. Morales-Guio, L.-A. Stern, and X. Hu, "Nanostructured hydrotreating catalysts for electrochemical hydrogen evolution," *Chemical Society Reviews*, vol. 43, no. 18, pp. 6555–6569, 2014.